Journal Pre-proof

Removal and Dispersal of Biofluid Films by Powered Medical Devices: Modelling Infectious Agent Spreading in Dentistry

Ian Eames, Francesco D'Aiuto, Somayeh Shahreza, Yousef Javanmardi, Ramanarayanan Balachandran, Martin Hyde, Yuan-Ling Ng, Kishor Gulabivala, Sara Watson, Hywel Davies, Nicolas Szita, Janette Khajeh, Jeanie Suvan, Emad Moeendarbary

PII: S2589-0042(21)01313-4

DOI: https://doi.org/10.1016/j.isci.2021.103344

Reference: ISCI 103344

To appear in: *ISCIENCE*

Received Date: 2 March 2021

Revised Date: 27 August 2021

Accepted Date: 22 October 2021

Please cite this article as: Eames, I., D'Aiuto, F., Shahreza, S., Javanmardi, Y., Balachandran, R., Hyde, M., Ng, Y.-L., Gulabivala, K., Watson, S., Davies, H., Szita, N., Khajeh, J., Suvan, J., Moeendarbary, E., Removal and Dispersal of Biofluid Films by Powered Medical Devices: Modelling Infectious Agent Spreading in Dentistry, *ISCIENCE* (2021), doi: https://doi.org/10.1016/j.isci.2021.103344.

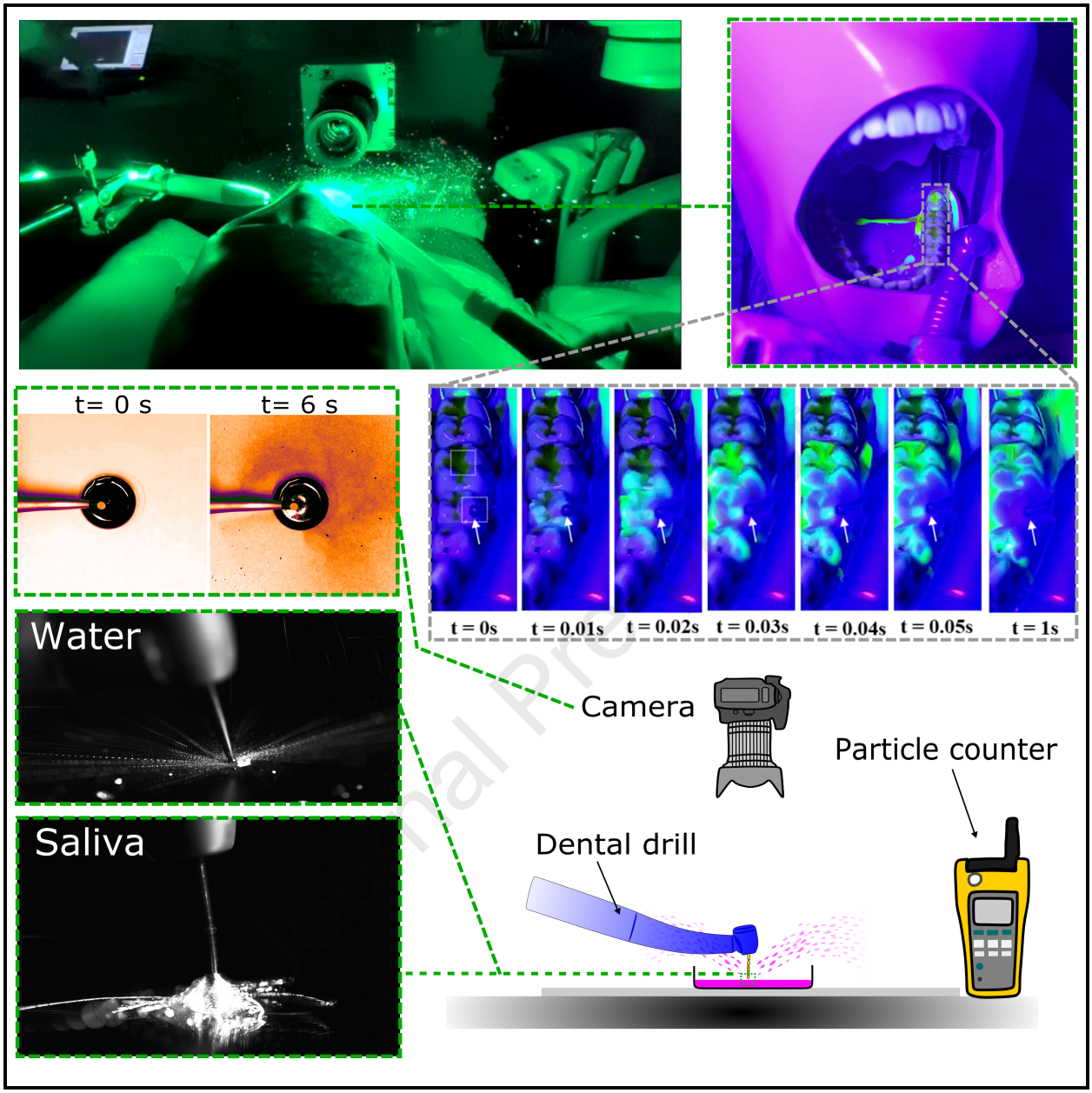
t= 0 s
t= 6 s
Water
Saliva
t = 0s
t = 0.01s
t = 0.02s
t = 0.03s
t = 0.04s
t = 0.05s
t = 1s
Camera
Particle counter
Dental drill

Removal and Dispersal of Biofluid Films by Powered Medical Devices: Modelling Infectious Agent Spreading in Dentistry

Ian Eames[1,*], Francesco D'Aiuto[2*], Somayeh Shahreza[1], Yousef Javanmardi[1], Ramanarayanan Balachandran[1], Martin Hyde[3], Yuan-Ling Ng[4], Kishor Gulabivala[4], Sara Watson[1], Hywel Davies[1],Nicolas Szita[5], Janette Khajeh[1], Jeanie Suvan[2,*], Emad Moeendarbary[1*]

[1]Department of Mechanical Engineering, University College London, Torrington Place, London, WC1E 7JE, UK
[2]Unit of Periodontology, UCL Eastman Dental Institute, University College London, UK
[3]TSI, 30 Millbank, Westminster, London SW1P 4WP, UK
[4]Unit of Endodontology, UCL Eastman Dental Institute, University College London, UK
[5]Department of Biochemical Engineering, University College London, Bernard Katz Building, Gower Street, London, WC1E 6BT, UK

*corresponding authors
Ian Eames, i.eames@ucl.ac.uk
Francesco D'Aiuto, f.daiuto@ucl.ac.uk
Jeanie Suvan, j.suvan@ucl.ac.uk
Emad Moeendarbary, e.moeendarbary@ucl.ac.uk

Lead contact: Emad Moeendarbary, e.moeendarbary@ucl.ac.uk

Keywords: aerosol-generating procedures (AGPs), disease transmission, droplets, infectious agents

Summary

Medical procedures can disperse infectious agents and spread disease. Particularly, dental procedures may pose a high risk of disease transmission as they use high-powered instruments operating within the oral cavity that may contain infectious microbiota or viruses. Here we assess the ability of powered dental devices in removing the biofluid films and identified mechanical, hydrodynamic, and aerodynamic forces as the main underlying mechanisms of removal and dispersal processes. Our results indicate that potentially infectious agents can be removed and dispersed immediately after dental instrument engagement with the adherent biofluid film while the degree of their dispersal is rapidly depleted due to removal of the source and dilution by the coolant water. We found that droplets, created by high-speed drill interactions typically travel ballistically while aerosol-laden air tends to flow as a current over surfaces. Our mechanistic investigation offers plausible routes for reducing the spread of infection during invasive medical procedures.

44

Introduction

Medical procedures using powered instruments span a broad spectrum of specialities including orthopaedics, otorhinolaryngology, ophthalmology, and dentistry, and have the potential to release biofluids into the local vicinity. While biofluids such as blood, saliva, mucous, or tears play various roles, such as nutrient conveyance, aid digestion and lubrication, they also have the potential to transmit viral and bacterial pathogens from one person to another (Xu et al., 2020). Several surgical procedures involve cutting bone or sinewy tissue, which demand a great deal of mechanical energy introduced either electrically or pneumatically. To mitigate tissue damage due to heat generated during cutting, coolant (usually water) is introduced continuously to quench the cutting surfaces. The presence of biofluids, water, air and moving surfaces in the form of instrument tips or blades creates a potential for dispersing infectious agents including splashes, aerosols (WELLS, 1934) and droplets and spreading infection through inhalation or a contact route (Tang et al., 2006).

While power-driven instrument types are common across clinical sciences, generally differing in their size and speed, dentistry represents a unique setting as it deals with the hardest tissues in the human body (i.e., enamel and dentine) requiring the fastest cutting drills and robust cooling mechanisms to prevent thermal damage to the dental pulp. Furthermore, the oral cavity, as the gateway to the body, is an open environment containing multiple biosolids and biofluids that serve as a reservoir for microbiota. The close connection with the respiratory tract and nasal pathway makes the oral environment and its associated biofluids potential reservoirs containing infectious agents that transmit diseases such as Mycobacterium tuberculosis, Herpes simplex or SARS-CoV-2.

The potential risk of spreading infection during a dental procedure involving an air-turbine drill and water coolant was recognised as early as the 1960's (STEVENS, 1963). The routes however by which infectious agents are removed and dispersed have not been thoroughly studied (Harrel and Molinari, 2004). The current understanding on this topic, encapsulated in international guidance WHO 2020, PHE 2020 ("COVID-19: infection prevention and control (IPC) - GOV.UK," n.d.), is that all instruments that create an aerosol require specialist protocols to mitigate the risk of spreading disease. The challenge of mitigating risk partly involves characterising what is in the air with some confusion over the definition of an aerosol. Typically an aerosol is characterised by particles whose diameter is less than 5 microns with the criterion based on the potential to be inhaled into the lower respiratory tract (Fennelly, 2020). The range for inhalation could be wider (less than 12 microns in diameter) and indeed a droplet size can shrink by as much as 80% due to evaporation. While, the guidance employs an instrument classification based on their power to generate aerosols, they lack the underpinning fundamental science of how instruments interact with biofluid films and their potential to generate agents carrying infection (Epstein et al., 2020).

Motivated by the lack of systematic investigation on the topic (Kumbargere Nagraj et al., 2020; Volgenant and de Soet, 2018), we studied how biofluid films, that may contain virus or bacteria, are removed and dispersed via dental instruments and procedures. We focus on the dispersal mechanism that is centred around the removal of biofluid films and crucially distinguish between coolant fluid that comes from the dental device and the potentially infectious fluid. Using imaging techniques and dyed fluid films, we analysed the fundamental mechanisms in a laboratory setting and assessed the relevant processes under clinically relevant conditions.

Results

Mechanisms of aerosol and droplet generation

Droplet size has an important consequence for transport processes. It is important to clarify the terminology applied to distinguish between the different droplet size. The usual way to distinguish

aerosols is based on the potential for deep inhalation setting a scale of 5 microns in diameter, rather than the physical processes that keep the matter in the air. Large droplets settle quickly and move ballistically while aerosols are distinguished by their long residence time in the air. The distinction between these two groups is imprecise, especially since droplets evaporate and shrink. Based on the resolution of our probing techniques, here we distinguish between aerosols, fine droplets and droplets corresponding approximately to <20 microns, <200 microns and >200 microns in diameter respectively. Application of airborne particle counter (detecting <20 μm particles), deposition (detecting >~50 μm particles), and high-speed imaging (detecting >~200 μm particles) techniques allowed us to probe the particles with sizes in these three categories.

We assessed three common dental devices (dental drill or air-rotor handpiece, ultrasonic scaler, 3-in-1 air-water syringe) for their potential to generate aerosols/ droplets by mechanical rotation/vibration of surfaces (bur or ultrasonic tip) or flow of air/water through small orifices (Fig 1a). Air-rotor generates the finest particles because of the fastest bur rotation and the highest air speed. Generated droplets are propelled ballistically, while the created aerosol cloud around the drill is dispersed by the air jet and the coolant spray generates a turbulent aerosol jet flow that slows rapidly with distance due to entrainment (Fig 1b-d). The droplets generated by an ultrasonic scaler appear to be larger and move typically with an average velocity of ~2 ms^{-1} (Fig 1b-d). The air-rotor handpiece propels droplets at a greater initial velocity compared to ultrasonic scaler (Fig 1b) with droplets reaching velocities of over ~10 ms^{-1} at proximity to the rotating bur. Close to the devices, the droplets travel in a linear path while far from the device, they move with a parabolic trajectory (Fig 1b).

The ability of the instrument to convert the coolant water into droplets of different sizes depends on the balance between the surface tension force and the inertial forces created through either of vibrating/rotating surfaces, air and water flow. The different strengths in the mechanical and aero/hydrodynamic forces lead to contrasting droplet sizes with aerosols/fine droplets tending to be generated from the fast-moving surfaces (bur of the air-rotor or vibrating tip of the ultrasonic scaler). Air flow jet (expelled from the air-rotor handpiece) create droplets while very large droplets are formed by the water jet (3-in-1 air-water syringe). We estimated the Weber number (We), which is a measure of the relative strength of inertial to surface tension forces, to characterise the potential of the instrument to generate droplets of different sizes. The ultrasonic scaler generates larger droplets, which splash when impacting surfaces (We=~20), while the air-rotor creates faster moving small droplets (We=~1.5), that have a greater tendency to follow the air flow (Fig 1e). Based on the type and strength of the inertial forces, we categorised the ability of the instruments to convert the coolant water into aerosols, fine droplets, and droplets on a diagram in Fig 1f (see Scaling analysis in the method section).

The inertial forces that involve in the generation of droplets from the coolant water similarly drive the removal of fluid film in the form of splashes, aerosols and droplets of different sizes. Therefore, as examined in the next sections, aerosols and droplets can be generated from the biofluid layer through either mechanical interactions caused by a surface vibrating or rotating while in contact with the layer, aerodynamic interactions caused by the air flowing onto the layer and hydrodynamic interactions caused by the flow of coolant water jet or droplets hitting the layer. To build up a conceptual picture of the removal processes, we designed a series of experiments starting with an idealised interaction with a fluid film and then building up to more complex interactions involving model teeth and mouth of a manikin.

Interaction of powered instruments and adherent layers in controlled setting

The first set of experiments involved the interaction between a fixed instrument and a fluid film focussing specifically on the air-rotor (Fig 2a), which produced the highest amount of aerosol and fine droplets with high velocity characteristic (Fig 1e). Furthermore, examination of the air-rotor and ultrasonic scaler interacting with a thin fluid layer placed on a circular glass slide clearly suggested the negligible droplet

generation by ultrasonic scaler compared to air-rotor particularly when operated at a fix position (SI Figs 2 and 3).

To distinguish between the interconnected removal mechanisms a fixed air-rotor was operated to run the drill, water, and coolant separately and its interaction with a thin layer of biofluid under three operating modes was examined; **mode-1**: the normal operating condition which involves rotation of the bur driven by the air jet while allowing the expulsion of both the air and coolant jet; **mode-2**: rotation of the bur driven by the air jet allowing the expulsion of the air while water expulsion was inhibited; and **mode-3**: rotation of the bur driven by the air jet while both air and water jet expulsion were inhibited.

Deposition measurements

Under these three modes and using dyed water (dyed either water film or coolant water), first we imaged the droplet deposition during continuous 2 min operation of the instrument engaging with a layer of water covering the bottom of a plastic dish (Fig 2a). Surprisingly, during the continuous operation in mode-1 and -2 no droplets and splashes were detected and only a limited number of splashes were observed immediately after operation was stopped in mode-1 (Movies 1-3). Interestingly, in the absence of air and water jets (mode-3), upon start of the bur rotation, the immediate interaction of the bur with the adherent fluid layer generated large splashes (Fig 2b, Movie 4). This was followed by a significant deposition of dyed droplets during the 2 min interaction of the bur with the dyed layer which generated a continuous cloud of fine aerosol deposited with distinct asymmetric patterns involving a complex interaction between the turbulent air flow induced by the bur and the gravity-driven flow induced by the aerosols (Fig 2b, first column). The intensity of the dye pattern increased in time due to the steady flow of aerosol-laden air. The aerosol-laden air appeared to flow over the edge of the dish while the lip of the dish perturbed the low-speed aerosol-laden flow and created a narrow shadow around the dish (Fig 2b).

Next, we dyed the coolant water instead and investigate the dispersal patterns generated as the result of water jet expulsion and the interaction of the drill with water jet and the clear/ undyed water film layer (Fig 2b, columns 2, 3 and 4, Movies 5-7). When the air-rotor was interacted with the clear layer under mode-1 (using dyed coolant water), significant deposition was observed (Fig 2b, second column) which was less pronounced compared to mode-3 (Fig 2b, first column). The removal of the water layer reduced the amount of deposition (Fig 2b, third column). However, very small amount of deposition (mostly located at the proximity to the lip of the dish) was detected when bur was removed (Fig 2b, last column).

Finally, investigation of the effects of layer thickness revealed that the intensity and the spread area of the deposition depend on the thickness of the layer when air-rotor was operating in mode-3 (Fig 2c). When the thin layer was engaged with the bur, the continuity of the dyed water layer was affected due to the removal of the water and limited amount of deposition was detectable (Fig 2c). However, when the thickness of the dyed layer increased a continuous reservoir of dyed water was available for removal/ droplet generation and therefore the deposition area was expanded due to a high mass flux of droplets and continuous flow of aerosol-laden current (Movies 8-10).

Aerosol measurements

Our simple photography technique was capable of capturing the dynamics of droplet (with diameters larger than ~50 μm) deposition and suggested distinctive removal and dispersion mechanisms. However, finer droplets (typically less than ~20 μm) are known to have a higher degree of retainment within the air and penetration into respiratory system making them more likely source of disease transmission. Therefore, we tested the validity of our findings for significantly finer particles by employing an airborne particle counter to probe the dispersal evolution of 0.3 to 10 μm droplets. Consistent with the deposition tests, no aerosolised droplets were detected under mode-2 (explusion of air without presence of coolant water) as the flow of air pushed the dyed layer away from the bur, preventing the

bur engagement with the water layer (Fig 2d). However, presence of aerosols was recorded under mode-1 and mode-3 when the bur was engaged with water jet or sufficiently thick fluid layer generating a significant flow of aerosolised droplets (Fig 2e,f).

These observations suggest that under mode (1) the aerosol (in the form of either infectious or non-infectious fine droplets) can be generated via three sources: the bur interacting with the primary layer (Drill interaction), the bur interacting with air/water jet that directly hitting the bur and also the dish (Air+Water+Drill), and the air/water jet direct dispersion or expulsion after hitting the dish (Air+Water). Our examination of the distinct contributions from each source to aerosol production (Fig 2e,f), indicated that Air+Water+Drill generated the highest levels of aerosol with a wide range of sizes (0.3 to 10 μm) that remained within the air beyond 2 mins operation, while the Air+Water produced significantly lower aerosol levels with almost negligible amount for 5 and 10 μm droplets (Fig 2e,f) consistent with deposition experiments (Fig 2b). Interestingly, compared to Air+Water+Drill, Drill condition produced significantly lower amounts of (potentially infectious) aerosol, which diminished rapidly. Furthermore, for each curve we observed an initial peak (occurring few seconds after the start of the operation) with the fastest peak occurring for the Drill, suggesting the significant inertial power of fast rotating bur and effects of pre-engagement and wetting of the bur with the biofluid film. Removal of water layer from the dish had minimal effects on production of small aerosols (0.3 μm, SI Fig 1d) while the amount of large aerosols (5 μm, SI Fig 1e) significantly increased under the presence of water layer which is consistent with the deposition measurement (Fig 2b, second and third columns).

Simultaneous measurements of aerosol at 0.4 m and 2 m distances (using two probes located on the same height) showed a lag of ~20 s in the occurrence of the peak at the further distance (Fig 2h) while the aerosol concentration decayed after ~60 s at both sites after the operation stopped (Fig 2h and SI Fig 1f-h). The concentration of aerosol at the further point was dramatically lower for large droplets, with the loading of 5 and 10 μm approached to almost zero.

High speed imaging

Conducting high speed imaging we also visualised the interaction of rotating bur with the thin fluid film and investigated how the fluid film is removed and aerosolised (Fig 3). Three stages of removal were revealed: the initial rotation of the burr, steady rotation with droplet generation and full removal of the film (Fig 3, Movies 11-16). During the initial rotation of the bur, the water was also rotated by the bur creating initial thin water filaments that fragmented and produced droplet ejecta whose size became progressively finer as the water layer diminished (Fig 3a). The ability of a bur to remove an adherent biofluid film depends on the rheological properties of the biofluid which was assessed by comparing the removal of water with unstimulated saliva collected from a participant (Fig 3b). While similar processes observed for both water and saliva layers, the timescale of the processes was longer for saliva layer. The saliva layer initially rotated around the bur at longer timescale, longer filaments were formed and fine droplet formation via fragmentation was greatly suppressed compared to water film due to increased viscosity (Fig 3b).

Interaction of powered instruments and adherent layers assessed in simulated clinical setting

To gain a more realistic insight relevant to the clinical situation, we next investigated the interaction between an air-rotor and teeth using either a set of adult teeth model or a manikin. Considering real tooth geometry meant that the bur and air-water flows interact with uneven/ rough surfaces and the concave section of the crown (a potential saliva reservoir) while the oral cavity has significant impact on containment of the splashes and the aerosol flow.

In the first series of tests (Fig 4a), teeth (44-47 ISO 3950) were coated with simulated saliva mixed with fluorescein dye, and an air-rotor handpiece was held by hand near the teeth with the bur contacting the occlusal surface of tooth 46 (ISO 3950). Upon turning on the air-rotor (within first 300 ms), the presence

of cooling water immediately diluted the fluorescein coating leading to the flow of dye mixture over and away from the teeth (Movie 17). The convex cusps of the crown created a pool of diluted dyed water pooling at the occlusal pit. Consistent with the tests in Fig 2b, engagement of the drill with the pooled dyed water led to generation and ejection of a small number of fine dyed droplets detected after ~1000ms at the distances up to ~20 cm away from the tooth (Fig 4a).

Next, the dispersion of the coolant water was examined by mixing the coolant water with the red food dye. The dyed coolant water initially coated the bur and the crown of the tooth before any observable droplet dispersion (Movie 18). Within 100 ms, we observed droplet deposition generated through mechanical and aero/hydrodynamic processes. The drill's mechanical interactions (via its shank similar to Fig 1a) with coolant aerosol-jet potentially generates aerosols with the smallest droplet size (Fig 1f) while the bur engagement with the coolant pool at the occlusal pit produces fine droplets (as observed in Fig 2c). The aerosol-laden coolant jet, inertially impacted the tooth surface and finer components dispersed in the air and flow as current along the surface (Movies 17,18).

Finally, using a manikin we explored the influence of drill orientation/movement and the mouth geometry in directing and confining droplet splatter. Simulant-saliva was mixed with fluorescein powder and applied to cover the teeth (34-38 ISO 3950) and the bur was engaged with teeth 35 on the buccal cusp. As soon as the air-rotor started, the simulant-saliva layer was rapidly removed from the teeth (in less than 1s) by the water jet before the bur engaged with the tooth (Fig 4c). While the water jet diluted the dyed simulant-saliva (as detected through increase in the fluorescent light intensity, Fig 4d), the movement of the drill along the buccal side and its engagement with the teeth surface led to a splatter outside the mouth (Fig 4e). Droplets (mostly generated aerodynamically by the coolant jet and mechanically by the bur) were propelled through the air with a tendency to be entrained into the vortex created by flow separation at the side of the manikin's mouth, leading to the deposition of a mixture of dyed and clear large droplets on the manikin face (Fig 4e). Thorough scrutinisation of all areas around the manikin indicated a discrete number of (<5) fluorescent splashes at distances up to 1 m from the head towards the foot. No dyed splashes were observed in the 4 settling plates placed within 50 cm of the manikin head while further examination of these plates with a fluorescent microscope revealed a small number of fine spots (Fig 4f). Owing to the absence of a propelled air component, the removal pattern changed dramatically with the ultrasonic scaler as the coolant water from the agitator simply flushed the simulant-saliva layer from the teeth and splashed around the mouth only when operated continuously over several teeth.

Finally, we assessed the degree of the suspension of fine droplets (up to 2.5 microns) in the air (Fig 4g) when either air-rotor or ultrasound scaler was operated in the manikin mouth by a dentist running a 3min routine dental procedure. We detected a rise of 120 $\mu g m^{-3}$ of PM2.5 (average value 50 $\mu g m^{-3}$) during the air-rotor operation and this level dropped dramatically when drilling ceased (10 minutes after the procedure was stopped, the mass loading dropped to 5 $\mu g m^{-3}$). During the ultrasonic scaler operation at a *fixed position* and directed into the mouth, the air sampler did not detect a significant change showing values below 3 $\mu g m^{-3}$ of PM2.5 (Fig 4g). However, when the ultrasonic scaler was swept around the mouth, and in some cases impinged on the air sampler (Fig 4f), the PM2.5 reached a maximum of 100 $\mu g m^{-3}$ (average of 30 $\mu g m^{-3}$). As soon as the procedure ceased, the measured particle loading in the air dropped rapidly back to the levels prior to the procedure starting and at a much faster rate than observed with the dental drill.

Discussion

The primary mode of disease transmission in the clinical setting is fluidic (Bourouiba, 2021), either through fine aerosols entering the air that can be inhaled, or through aerosols, fine droplets and splashes that settle on surfaces and are transferred via contact (Peng et al., 2020; Tang et al., 2006). Infectious agents spread by medical devices affix those generated by normal pathways (Fig 5a) including

breathing, speaking, coughing and sneezing (Abkarian et al., 2020). The powered medical procedures and especially dental operations (as they use high powered instruments) involve complex interactions between fast-moving surfaces, air and water jets that make the assessment of the risk of the spread of infectious materials from patient to medical practitioners due to medical procedures challenging (Fig 5a).

Numerous studies have analysed the potential risk of disease transmission by aerosol and splatter associated with dental procedures. Splatter tests with dyed water coolant show spray deposition over large distances (Harrel et al., 1998) with a range of droplet sizes deposited within 2 m and aerosols potentially dispersed further (Allison et al., 2020). CFU microbiological assays have provided overwhelming evidence that the use of air rotors and drills enhances the spread of bacteria from the mouth compared to when transported away from the patient through breathing, speaking, or coughing (Rautemaa et al., 2006). Many previous studies do not distinguish between the clean splashes/ droplets/ aerosols (ejected directly from the devices (Sergis et al., 2020) or indirectly through interaction of ejected clean flow with other surfaces) and those that contain the infectious biomaterials (mostly generated from removal of infectious biofluid films). More recent studies have attempted to measure the distribution of aerosolised simulant-saliva laden with a virus or bacteria (such as *Streptococcus mutans*) that were continuously introduced into a phantom head mouth, while powered devices were operated on the teeth (Ionescu et al., 2020; Vernon et al., 2021). Vernon et al (Vernon et al., 2021) analysed the influence of mitigation strategies (such as rubber dam and aspiration) on aerosol loading and CFU on settling plates, and contrasted the spread from high-speed air rotors with lower speed electric drills. While these quantitative measurements highlighted the importance of drill speed, air and availability of saliva on the dispersal process (Holliday et al., 2021) the exact mechanisms by which infectious agents are removed and subsequently dispersed were not thoroughly analysed.

The airborne spread of infection is fluidic in nature and relies on how infectious materials that are mostly embedded within adherent biofluid films are removed, enter the air and are being dispersed. Therefore, assessing the risk of disease transmission from powered medical instruments first requires a thorough understanding of the removal and dispersal processes that are involved during instrument interaction with adherent biofluid films. Indeed, the small size of bacteria and especially viruses compared to a large body of fluid means that they move with the fluid and as such, tracking the fluid can provide an appropriate proxy for following transport of infectious agents. Consequently, analysis of the removal and dispersal of the adherent biofluid films using dye techniques or airborne particle counters (as in our study) can provide a valid approximation to evaluate the spatiotemporal spread of infectious agents.

Our laboratory tests identified three independent mechanisms for removing biofluid films: mechanical due to vibrating/rotating surfaces, aerodynamic caused by air flow and hydrodynamic caused by water flow or droplet impact. Our bright-field visualisations of the deposition and aerosol measurements (Figs 2 and 4), support the view that the aerosol cloud generated during dental procedures mostly flow as a current (with and estimated velocity of ~0.08 m/s) and continuously settles, as it moves along the surface and is not dispersed randomly unless there exists turbulence in the air (generated externally for example by ventilation systems or the movement of people).

Our data confirmed that the operation of the air-rotor has the higher ability to potentially remove and disperse the infectious agents (Fig 1, SI Figs 2, 3). As summarised in Fig 5b, three different mechanisms appear during the operation of an air-rotor with the high-speed rotation of the bur and its interaction with film having the greatest potential for film removal and the subsequent dispersal. Depending on the geometrical constraints and operational orientation, the three mechanisms may engage with each other in an additive or subtractive fashion to remove and disperse potentially infectious biofluid film. For instance, when the bur interacts with a flat surface (Fig 2), the air flow may act to deplete the fluid film or reduce the thickness of the fluid film near at the bur which decreases the amount of potentially infectious biofluid to be exposed to the drill and turn to fine aerosols through mechanical interactions.

However, when the bur is located in an occlusal pit (Fig 4), the air flow may enhance the removal process and splash generation by exerting high shear forces on the film and particularly at the cusp of the teeth edge (Fig 5c). Furthermore, while we designed the experimental configurations to enhance the removal of the biofluid film coating the teeth, only a small fraction of the adherent layer was observed to be removed and deposited over a short distance (Fig 5c).

There is a growing number of practical methods to reduce the potential of infectious agents spread in dentistry, including reducing the availability of biofluids through the use of dams (Fine et al., 1993), application of suction devices to remove aerosol-laden close to the point of generation (Vernon et al., 2021). Hassandarvish et al (Hassandarvish et al., 2020) have shown that mouthwash can reduce viral load in biofluids in a laboratory setting. Previous measurements reported the viscosity of the human saliva to be at least twice the water viscosity (CE et al., 2000). Consequently, our experiments on the human saliva (Fig 3b) indicate that increasing the viscosity of a biofluid (by replacing water with human saliva) suppresses removal mechanisms, which are especially important during the start of drilling. Other groups have suggested changing the rheological properties of the coolant water to reduce aerosolisation (Plog et al., 2020). Therefore, manipulating the rheological properties of the fluids (biofluids and coolants) involved during powered medical procedure are among other possible ways to suppress the aerosol generation.

In summary, our work provided a mechanistic view of the general processes of biofluid film removal and dispersal by powered medical devices, specifically in the context of dentistry. This provides an important steppingstone to understand and propose mitigation strategies to reduce the risk of the spread of airborne infection.

Limitations of study

Our study focuses on modelling infectious agent spreading employing the dye technique and thus no specific microbiota or virus was used in our study. However, one limitation of such techniques is their inability to predict the levels of infectivity of the dispersed biofluid precisely. Indeed, infectious agents embedded within the fluid body may get inactivated by heat or mechanical forces generated in drilling or desiccation following droplet evaporation.

Acknowledgements
The authors wish to thank the UCL Covid-19 Rapid Response Fund for supporting the research in the paper through the project “Reducing the risk of aerosols in dentistry and getting dentists back drilling”. The project benefited from the generous equipment loan of dental instruments by NSK and assistance from Mark Beckwith. Peter Kelly, Professor Yannis Ventikos from UCL Mechanical Engineering and Professor Stephen Porter from Eastman Dental Institute facilitated early access to laboratory and clinal settings. We would like to acknowledge that contribution of this work was undertaken at UCLH/UCL who received a proportion of funding from the Department of Health’s NIHR Biomedical Research Centre funding scheme. SS, YJ and EM are grateful for financial support by Leverhulme Trust Research Project Grant (RPG-2018-443), the Cancer Research UK Multidisciplinary Award (C57744/A22057) and Biotechnology and Biological Sciences Research Council Grant (BB/V001418/1) to EM.

Author contributions
IE and EM designed and performed the majority of the experiments. RB, MH and HD helped with laser sheet imaging. FD, YLN, KG, JK and JS helped with the clinical setting experiments. SS, SW and NS helped with laboratory setting experiments. EM analysed the data with helps from IE and YJ. IE and EM wrote the manuscript with contributions from FD, YJ and JS. All authors discussed the results and commented on the manuscript.

Declaration of interests

409 The authors declare no competing interests.

Figure titles and legends

Figure 1 Droplet generation capacity of different dental devices.
(a) High speed photography (5000 frames per s) of aerosol and droplets showing an instantaneous view (left images) and a maximum projection (right images) of 100 image sequences (corresponding to 20 ms) highlighting the trajectory of the dispersed phase. The panels (from top to bottom) correspond to air-rotor, air-rotor (without burr), low-speed drill with external 3-in-1 coolant jet and back-exhaust, ultrasonic scaler, low-speed drill and 3-in-1. The red, green and blue arrows show regions that aerosols (<20 microns), fine droplets (20-200 microns) and droplets (>200 microns) were generated, respectively. **(b)** Characterization of the spray dynamics for air-rotor (left panel) and ultrasonic scaler (right panel). The velocity contours were estimated by tracking individual droplets using PTV. Scale =1 cm. **(c,d)** The distribution of droplet diameter and speed for the air-rotor and ultrasonic scaler. **(e)** The size and velocity of individual particles were combined to estimate the distribution of the Weber number. **(f)** Regime diagram showing the characterisation of different dental instruments according to their potential to generate aerosols, fine droplets and droplets expressed through the movement of a liquid jet (II_1) or by mechanical agitation (II_2). The inset images are taken from the regions specified by red, green and blue squares in (a).

Figure 2 Removal and dispersion of the adherent biofluid film in laboratory setting.
(a) Schematic of the laboratory setup used to analyse the mechanisms of layer removal with photos taken from the above and the air sampler located 40 cm away from the dish. **(b)** Top view images showing the temporal evolution of dye deposition (from either dyed coolant water or dyed fluid layer) due to air-rotor handpiece operating under different modes. Scale=10 cm. **(c)** Effects of fluid layer thickness on the temporal evolution of dye deposition due to a drill engaging with the layer. Scale=10 cm. Arrows in (b) and (c) point to the regions that small amount of deposition was detected. **(d-g)** Air particle count (sampled continuously over 5 min at 40 cm distance from the drill by a particle counter that measured cumulative particle count every 5s in 0.2 liters of air) as a function of time and under a variety of drill-air-water configurations. To estimate the baseline, the particle counter ran for 0.5 min prior to the operation of the drill. Then while particle counter was continuously running, the air-rotor handpiece was operated for 2 min. After the drill operation was stopped, the particle counter was kept running for additional 2.5 min. **(d)** Measurements of air particle counts (0.3μm and 5μm inset) when air-rotor was operated on a thick layer of water film under three operating condition of air only (mode-2 but without the drill), drill with air only (mode-2) and drill only (mode-3). **(e,f)** Measurements of air particle counts (0.3 μm in (e) and 5μm in (f)) when air-rotor was operated on a layer of water film under three operating condition of drill only (mode-3), air with water only (mode-1 but without drill) and drill with air and water (mode-1). The insets are the zoom of the first 1.5 min. **(g)** Influence of the layer thickness on 0.3 μm particle count (5 μm inset) in mode-3 (drill rotation with inhibited expulsion of air and water). **(h)** Simultaneous measurements of particle count (0.3μm) at 0.4m and 2.0m from drill only (see SI Fig 1f for 5μm particles and SI Figs 1g-h for individual unaveraged curves). The curves in (d and g) are the smoothed data from individual measurements representing the trend. The curves in (e), (f) and (h) are the smoothened, averaged of data from three independent experiments with shades indicating the standard error.

Figure 3: The dynamics of biofluid film removal and influence of fluid properties.
(a,b) High-speed images (7000 frames per s) capturing the dynamics of bur rotating at ~20000 rad/s and engaging with water or unstimulated saliva (from a human participant) droplet/film. In (**a,b**), the top images are the instantaneous single snapshots, the middle images were created by overlaying single snapshots over a period of time. The bottom images were created by colour coding single snapshots and overlaying on top of one another. **(a)** The removal of a droplet of water (~ 2 mm in diameter) collated

in three sequences: acceleration of bur (0-0.055s), steady full-speed rotation of bur (0.085-0.13s), leading to full removal of droplet/film (0.14-0.195s). Scale=5 mm. **(b)** The interaction of a thin film of saliva (~500 µm thickness) with bur is shown at different stages (0-0.22s, 0.300-0.52s and 0.86-1.08s) after the start of the drill rotation at t=0. Scale=5 mm.

Figure 4: Assessment of biofluid film removal and dispersal in clinically relevant conditions.
(a) The removal of a fluorescently dyed simulated saliva layer by an air-rotor handpiece operating on model teeth. The teeth (45-47 ISO 3950) were coated with dye, the drill engaged with tooth 46 and the coolant water was undyed. Using fluorescent lamp, the dyed droplet splatters were detected up to 10 cm away from the model teeth. The blue arrow points to the regions of undyed water deposition and the yellow arrows indicate the regions that dyed flow or small deposition could be detected. Scale=1 cm. (**b**) The dispersal of coolant water (dyed with red food colouring) from air-rota handpiece operating on model teeth. Arrows point to the regions that small amount of deposition could be detected. **(c-g)** Measurements conducted in a simulated clinical setting with a dentist who performed procedures on a phantom head (located on a dental chair). The air-rotor handpiece pointed at the buccal cusp of the occlusal surface of teeth 35, while teeth 34-38 were coated with fluorescently dyed simulant saliva layer. **(c)** Image sequences show the dilution of the simulant saliva loaded with fluorescein dye. The arrows point to the tip of the bur. Scale= 1 cm. **(d)** Intensity profiles at two locations on the teeth (areas located close to the tip and ~ 1 cm away from the tip) rapidly decayed due to dilution by the coolant water. **(e)** The local splatter pattern imaged on the surface of the manikin's face (located ~20 cm away from drilling point) after a 3 min continuous drilling procedure. **(f)** A small number of fluorescent particles (around ~200 µm diameter) were detected in areas up to 0.5 m away from the drilling point. Fluorescent imaging was used to scan the tracer Petri dishes distributed up to 2m away from the head. Scale=1 mm. **(g)** Total mass loading in the air for sub 2.5 micron particles during the operation of either air-rota handpiece in fixed position or the ultrasonic scaler operating in fixed/ static or moving conditions. The inset is the zoom of the dotted area.

Figure 5: Summary of the potential risks involved in transmission of infectious agents and the critical mechanisms for the removal and dispersal by powered instruments in dentistry.
(a) Collage showing the production of aerosols and droplets by powered mechanical devices in the dental setting and their link through contact and airborne transmission routes. **(b)** Insert images show the influence of either drill, drill/air and drill/air/water on the removing dyed simulant saliva. Schematic shows the removal of adherent layers through three mechanisms: mechanical (moving or vibrating surface), aerodynamic (due to the air movement) and hydrodynamic (impact of droplets or movement of water). Color contours and arrows show the qualitative comparison between the levels of the shear stresses generated by different mechanisms. **(c)** The interaction between an air-rota and teeth covered with dyed simulant saliva under conditions of drill, drill+air and drill+air+water. These panel were used as insets in (b).

Movies 1-10: Top view videos (related to Figure 2) showing the interaction of air-rotor with a water layer.
Mode-1: The normal operating condition which involves rotation of the bur driven by the air jet while allowing the expulsion of both the air and coolant jet.
Mode-2: Rotation of the bur driven by the air jet allowing the expulsion of the air while water expulsion was inhibited.
Mode-3: Rotation of the bur driven by the air jet while both air and water jet expulsion were inhibited.

Investigating effects of air flow:
Movie 1: Operation in mode-2 but with removed bur on dyed layer.
Movie 2: Operation in mode-2 on dyed layer.
Movie 3: Operation in full condition (mode-1) on dyed layer.

Investigating droplet splashes from water/air jet:
Movie 4: Operation of drill only (mode-3) on dyed film (~3mm thickness).
Movie 5: Operation in full condition (mode-1) with the flow of dyed water on undyed layer (~3mm thickness).
Movie 6: Operation in full condition (mode-1) with the flow of dyed water on dish with no water layer.
Movie 7: Operation in mode-1 but with removed bur and flow of dyed water on undyed layer (~3mm thickness).

Investigating effects of layer thickness:
Movie 8: Operation of drill only (mode-3) on thin dyed water layer (less than ~0.5mm thickness).
Movie 9: Operation of drill only (mode-3) on medium dyed water layer (~1mm thickness).
Movie 10: Operation of drill only (mode-3) on thick dyed water layer (~4mm thickness).

Movies 11-16: Videos (taken with high-speed camera) of the burr engaging with water (movies 11-13, Fig 3a) or unstimulated saliva collected from human participant (movies 14-16, Fig 3b) droplet/ film**.**

Movie 17: Video of the interaction of the air-rotor (operating in mode-1) with model teeth coated with fluorescent dye. The video was taken using fluorescent lamp.
Movie 18: Video of the interaction of the air-rotor (operating in mode-1 and the coolant water dyed by high concentration of food dye) with model teeth. The video was taken using a bright field light.

STAR Methods

Resource availability

Lead contact

Further information and requests for resources and data should be directed to the lead contact, Professor Emad Moeendarbary (e.moeendarbary@ucl.ac.uk).

Materials availability

This study did not generate new unique reagents.

Data and Code Availability

Additional Supplemental Items are available from Mendeley Data at https://dx.doi.org/10.17632/v9px86xh8w.1 or https://data.mendeley.com/v1/datasets/v9px86xh8w/draft?a=553d231d-9f66-46fa-b0d0-d50c3695d716

Experimental Model and Subject Details

No experimental model or human subject was used in this study.

Method details

The experimental tests were performed at the Royal National ENT and Eastman Dental Hospitals, UCLH. Two identical dental suites were used for the tests, with each serviced by clean air entry of 10 air-changes per hour (ACH) giving a potential air replenishment time of 6 minutes. Assessments in a simulated clinical setting were conducted on a phantom head with upper and lower dental arch containing 32 teeth. For the laboratory tests (performed in the UCL Environmental Fluid Mechanics Laboratory, Roberts Building), the instruments were analysed in isolation on a surface adjacent to a dental chair. The instruments used in this study are listed in SI Table 1.

Brightfield imaging

For the analysis of the sprays in Fig 1a, the instruments were held in position over a sink, illuminated with strong diffuse lighting and recorded using a high-speed CMOS camera colour camera (Phantom VEO710, Photron Inc, US). The images were recorded at a rate of 5000-7500 frames per second.

For imaging dynamics of biofluid film removal (Fig 3), approximately 100-200 µl of either water or the unstimulated saliva
collected from the human participant was laid on a flat metallic surface using small pipette tip. The interaction of the drill with the water or saliva layer was investigated using high speed camera (Phantom VEO710, Photron Inc, US) with the imaging speed of 5000-7500 frames per second. The procedure of unstimulated saliva collection involves resisting the swallowing of the participant's saliva and spitting into a small test tube every 20s for 2 min to collect approximately 2ml saliva.

Laser sheet imaging

Spray dynamics in Fig 1b was captured using laser illuminated Mie scattering technique with a laser vertical plane bisecting the dental instrument cross-section. This technique leads to capturing a much lower aerosol/droplet density in the image and is capable of measuring the velocity of individual droplets. High speed imaging of the spray was carried out using a 1000 mW, 515.3nm continuous diode laser (Genesis MX514-1000 SLM OPS Laser-Diode System) and a high-speed CMOS camera. The camera was fitted with a 100 mm lens producing an imaging window size varying from 60 x 100 mm to 30 x 50 mm. The images were captured at a frame rate of 5000-7500 Hz. The region of interest was set to observe the near field spray characteristics. An ultrasonic scaler, high speed air-driven drill and 3-in-1

air-water syringe were used to generate sprays. TSI Insight 4G software was utilised to capture the images.

Fluorescein imaging

The very small size of the viruses and low diffusivity of bacteria within a body of fluid mean that a dye model is an appropriate tool for tracking the infectious biofluid transport. Furthermore, the dye technique affords high spatial resolution in terms of tracking which enables the mechanistic view of the dispersal processes to be unpicked.

To examine the mechanism of saliva removal, a series of tests were performed using a phantom head. A simulant saliva (Biotene Oral Balance) was well-mixed with sodium fluorescein salt (0.625 mg/ml in simulant-saliva), applied over the teeth and illuminated using a UV lamp. Two types of fluorescein tests were applied. In the first, dyed simulant-saliva was applied to the teeth (34-38 ISO 3950) of a manikin by a dentist and an NSK air-rotor applied to tooth 35 with the drill in contact with the buccal cusp of the occlusal surface. The drill was applied at about 30 degrees from the horizontal. In the second, dyed simulant-saliva was applied to teeth 45-47 of a full-teeth model and an air-rotor applied to the occlusal surface of teeth 46 by an experimental professor. The air-rotor was aligned 10 degrees from the vertical plane.

The fluorescein salt concentration was initially extremely high that it absorbed light when applied to the teeth (appeared as dark green), but strongly fluoresced during dilution and in the presence of UV light. To capture the potential for simulant-saliva removal, a series of petri dishes were placed at distances 20, 40 and 80 cm from the head (in the chest direction) and 40 cm above the head. All the dishes were in the same plane. Prior to each test, the lids of the dishes were removed and replaced 10 minutes after the test started. Each test consisted of 200s continuous operation of the instruments. Photographs and videos of the experiments were recorded and analysed after the tests. During these tests, air was monitored for aerosol concentration PM2.5 and PM10 using a Temtop M2000 (Elitech) which was placed next to the phantom head. During the tests, 4 people present in the room to control the various components of the experiments.

Deposition tests

Splatter tests involved the interaction between powered instrument and a layer of fluid (water in Fig 2 or simulant saliva in Figs 4 and 5). The instrument was held in position and in contact with the centre of a 60 mm petri dish, placed onto a A0 sheet of white craft paper and a camera affixed above tests. Either the coolant water or the water layer was dyed using rhodamine dye (Merck Life Science, UK) and illuminated by a diffuse light source. Continuous videos were taken using a visualiser (IPEVO V4K Ultra HD) installed on top of the instrument.

Air sampling

During the fluorescein imaging tests within the hospital, air was sampled for a period of 10 minutes using a Temtop M2000 (Elitech). The device was placed adjacent to the phantom head and at the same level as the settling plates. The PM2.5, PM10 and particle count levels were recorded during the tests and for periods after the tests. Ventilation brought filtered air into the room and the 10 ACH for the room meant that the air born particle load was low; therefore, there is no need for the bassline subtraction and the raw data is plotted in Fig 4g.

During the splatter deposition tests in the laboratory, air was sampled using two Fluke 985 (Fluke, US) airborne particle counters that were placed flat on a workbench (pointing towards the petri dish) with a distance of 0.4 m and 2.0 m away from the dish. The ventilation system delivered unfiltered air to the laboratory (Roberts Building, UCL) and the additional components due to the local sources of aerosols was eliminated by subtracting the background concentration (SI Fig 1).

Quantification, reproducibility and image analysis

Experiments were repeated at least three times and plots and images are representative of at least three independent tests. For experiments in Figs 2e,f,h, the curves from three independent experiments were smoothened then averaged and the standard error was calculated as indicated by the shades. Individual curves related to effects of distance is presented in SI Fig. S1 g, h, which show the lag time due to distance more clearly. Quantification and plotting were performed in MATLAB (Mathworks) or Origin (OriginLab). Commercially available software, Imaris (BitPlane, South Windsor, CT, USA), was used to analyse the images. After optimising image volume rendering, spot object tools were employed to automatically segment and track the droplets. An autoregressive algorithm with a maximum inter-frame distance of 150 μm and a gap size of 3 μm was used to calculate the position of spots over time. The droplet sizes was analysed using the 'Analyse Particle' plugin in ImageJ (National Institutes of Health, USA); this technique was capable of identifying droplet size above 200 microns. The data was plotted using MATLAB.

Scaling analysis

The disruption of a water/air interface through mechanical agitation via a bur or vibrating tip or flow through a nozzle leads to droplets. The potential for generating an aerosol (<50 μm), fine droplets (50 to 200 μm) or droplets (>200 μm) depends on the magnitude of the forces that act on the water films and jets and this potential was assessed prior to the experimental study. For a water jet issuing from a hole with diameter H, at a speed U_J moving through air, the inertial force of the fluid is ρU_J^2. The potential for generating large droplets can be assessed by a characteristic measure based on comparing the surface tension (σ) that stabilises a droplet, and inertial forces, that destabilise the droplet: $\Pi_1 = \frac{\sigma}{\rho U_J^2 H}$, where ρ is the density of fluid This measure is the inverse of the Weber number. When the flow is slow and inertial forces are weak, Π_1 is large and millimetric droplets are created. When the flow is fast and inertial forces are large compared to surface tension force, Π_1 is small and an aerosol will be generated. For moving surfaces with angular velocity ω and length scale δ, a centrifugal acceleration on an adherent water films scales as $\omega^2\delta$ and a nominal centrifugal force $\rho\omega^2\delta^2$ giving a second dimensionless measure $= \frac{\sigma}{\rho\omega^2\delta^3}$. The equivalent measure for an instrument vibrating with a frequency Ω and displacement of the surface Δ is $\Pi_2 = \frac{\sigma}{\rho\Omega^2\Delta^3}$. The typical surface displacement measurement of 30 μm (Lea et al., 2002). The measures II_1 and II_2 form a discriminatory measure and a comparative measure between different instruments of their potential to generate aerosols and droplets.

Quantification and statistical analysis

Figures represent averaged or representative results of multiple independent experiments or simulations. The method section provides details concerning the number of independent experiments. Analyses were performed using data analysis toolbox in Microsoft Excel or Origin.

References

Abkarian, M., Mendez, S., Xue, N., Yang, F., Stone, H.A., 2020. Speech can produce jet-like transport relevant to asymptomatic spreading of virus. Proc. Natl. Acad. Sci. U. S. A. 117, 25237–25245. https://doi.org/10.1073/pnas.2012156117

Allison, J.R., Currie, C.C., Edwards, D.C., Bowes, C., Coulter, J., Pickering, K., Kozhevnikova, E., Durham, J., Nile, C.J., Jakubovics, N., Rostami, N., Holliday, R., 2020. Evaluating aerosol and splatter following dental procedures: Addressing new challenges for oral health care and rehabilitation. J. Oral Rehabil. joor.13098. https://doi.org/10.1111/joor.13098

Bourouiba, L., 2021. The Fluid Dynamics of Disease Transmission. Annu. Rev. Fluid Mech. https://doi.org/10.1146/annurev-fluid-060220-113712

CE, C., L, L., T, A., 2000. Film-forming properties and viscosities of saliva substitutes and human whole saliva. Eur. J. Oral Sci. 108, 418–425. https://doi.org/10.1034/J.1600-0722.2000.108005418.X

COVID-19: infection prevention and control (IPC) - GOV.UK [WWW Document], n.d.

Epstein, J.B., Chow, K., Mathias, R., 2020. Dental procedure aerosols and COVID-19. Lancet Infect. Dis. https://doi.org/10.1016/S1473-3099(20)30636-8

Fennelly, K.P., 2020. Particle sizes of infectious aerosols: implications for infection control. Lancet Respir. Med. https://doi.org/10.1016/S2213-2600(20)30323-4

Fine, D.H., Yip, J., Furgang, D., Barnett, M.L., Olshan, A.M., Vincent, J., 1993. Reducing bacteria in dental aerosols: pre-procedural use of an antiseptic mouthrinse. J. Am. Dent. Assoc. 124, 56–58. https://doi.org/10.14219/jada.archive.1993.0122

Harrel, S.K., Barnes, J.B., Rivera-Hidalgo, F., 1998. Aerosol and Splatter Contamination from the Operative Site during Ultrasonic Scaling. J. Am. Dent. Assoc. 129, 1241–1249. https://doi.org/10.14219/jada.archive.1998.0421

Harrel, S.K., Molinari, J., 2004. Aerosols and splatter in dentistry: A brief review of the literature and infection control implications. J. Am. Dent. Assoc. 135, 429–437. https://doi.org/10.14219/jada.archive.2004.0207

Hassandarvish, P., Tiong, V., Mohamed, N.A., Arumugam, H., Ananthanarayanan, A., Qasuri, M., Hadjiat, Y., Abubakar, S., 2020. In vitro virucidal activity of povidone iodine gargle and mouthwash against SARS-CoV-2: implications for dental practice. Br. Dent. J. 1–4. https://doi.org/10.1038/s41415-020-2402-0

Holliday, R., JR, A., CC, C., DC, E., C, B., K, P., S, R., J, D., J, L., N, R., J, C., C, N., N, J., 2021. Evaluating contaminated dental aerosol and splatter in an open plan clinic environment: Implications for the COVID-19 pandemic. J. Dent. 105. https://doi.org/10.1016/J.JDENT.2020.103565

Ionescu, A.C., Cagetti, M.G., Ferracane, J.L., Garcia-Godoy, F., Brambilla, E., 2020. Topographic aspects of airborne contamination caused by the use of dental handpieces in the operative environment. J. Am. Dent. Assoc. 151, 660–667. https://doi.org/10.1016/j.adaj.2020.06.002

Kumbargere Nagraj, S., Eachempati, P., Paisi, M., Nasser, M., Sivaramakrishnan, G., Verbeek, J.H., 2020. Interventions to reduce contaminated aerosols produced during dental procedures for preventing infectious diseases. Cochrane database Syst. Rev. 10, CD013686. https://doi.org/10.1002/14651858.CD013686.pub2

Lea, S.C., Landini, G., Walmsley, A.D., 2002. Vibration characteristics of ultrasonic scalers assessed with scanning laser vibrometry. J. Dent. 30, 147–151. https://doi.org/10.1016/S0300-5712(02)00009-X

Peng, X., Xu, X., Li, Y., Cheng, L., Zhou, X., Ren, B., 2020. Transmission routes of 2019-nCoV and controls in dental practice. Int. J. Oral Sci. https://doi.org/10.1038/s41368-020-0075-9

Plog, J., Dias, Y.J., Mashayek, F., Cooper, L.F., Yarin, A.L., 2020. Reopening dentistry after COVID-19: Complete suppression of aerosolization in dental procedures by viscoelastic Medusa Gorgo. Phys. Fluids 32, 083111. https://doi.org/10.1063/5.0021476

Rautemaa, R., Nordberg, A., Wuolijoki-Saaristo, K., Meurman, J.H., 2006. Bacterial aerosols in dental practice - a potential hospital infection problem? J. Hosp. Infect. 64, 76–81. https://doi.org/10.1016/j.jhin.2006.04.011

Sergis, A., Wade, W.G., Gallagher, J.E., Morrell, A.P., Patel, S., Dickinson, C.M., Nizarali, N., Whaites, E., Johnson, J., Addison, O., Hardalupas, Y., 2020. Mechanisms of Atomization from Rotary Dental Instruments and Its Mitigation. J. Dent. Res. 002203452097964. https://doi.org/10.1177/0022034520979644

STEVENS, R.E., 1963. Preliminary study--air contamination with microorganisms during use of air turbine handpieces. J. Am. Dent. Assoc. 66, 237–239. https://doi.org/10.14219/jada.archive.1963.0038

Tang, J.W., Li, Y., Eames, I., Chan, P.K.S., Ridgway, G.L., 2006. Factors involved in the aerosol transmission of infection and control of ventilation in healthcare premises. J. Hosp. Infect. https://doi.org/10.1016/j.jhin.2006.05.022

Vernon, J.J., Black, E.V.I., Dennis, T., Devine, D.A., Fletcher, L., Wood, D.J., Nattress, B.R., 2021. Dental mitigation strategies to reduce aerosolization of SARS-CoV-2 1 2. medRxiv 2021.03.24.21254254. https://doi.org/10.1101/2021.03.24.21254254

Volgenant, C.M.C., de Soet, J.J., 2018. Cross-transmission in the Dental Office: Does This Make You Ill? Curr. Oral Heal. Reports 5, 221–228. https://doi.org/10.1007/s40496-018-0201-3

WELLS, W.F., 1934. ON AIR-BORNE INFECTION*. Am. J. Epidemiol. 20, 611–618. https://doi.org/10.1093/oxfordjournals.aje.a118097

Xu, R., Cui, B., Duan, X., Zhang, P., Zhou, X., Yuan, Q., 2020. Saliva: potential diagnostic value and transmission of 2019-nCoV. Int. J. Oral Sci. https://doi.org/10.1038/s41368-020-0080-z

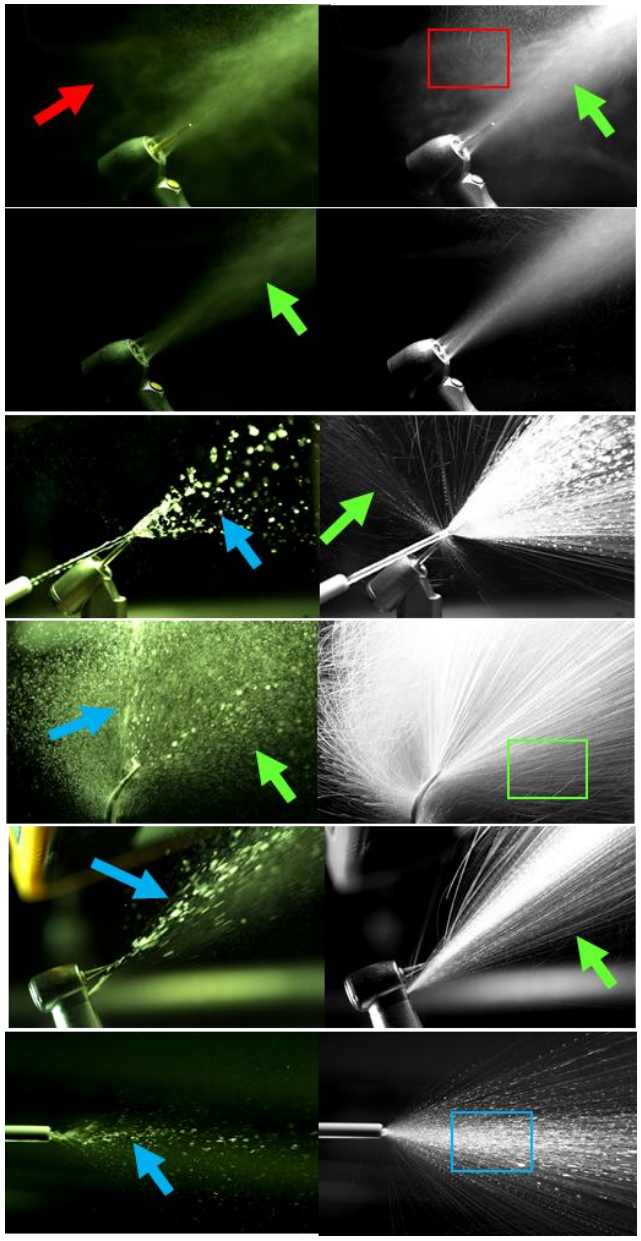

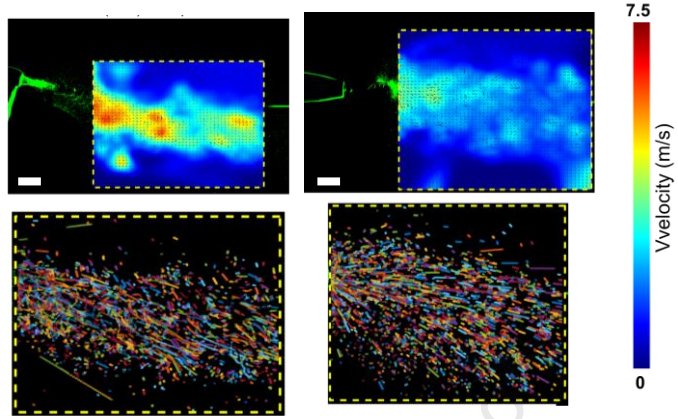

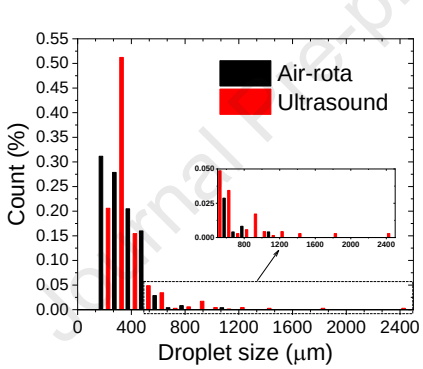

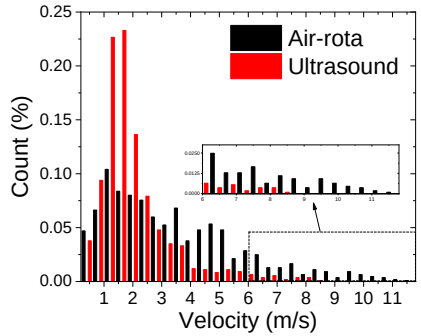

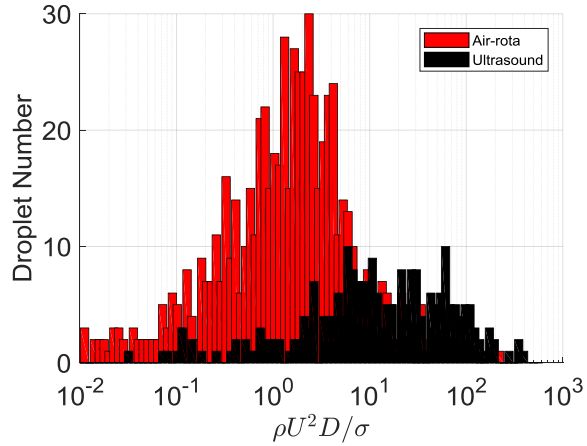

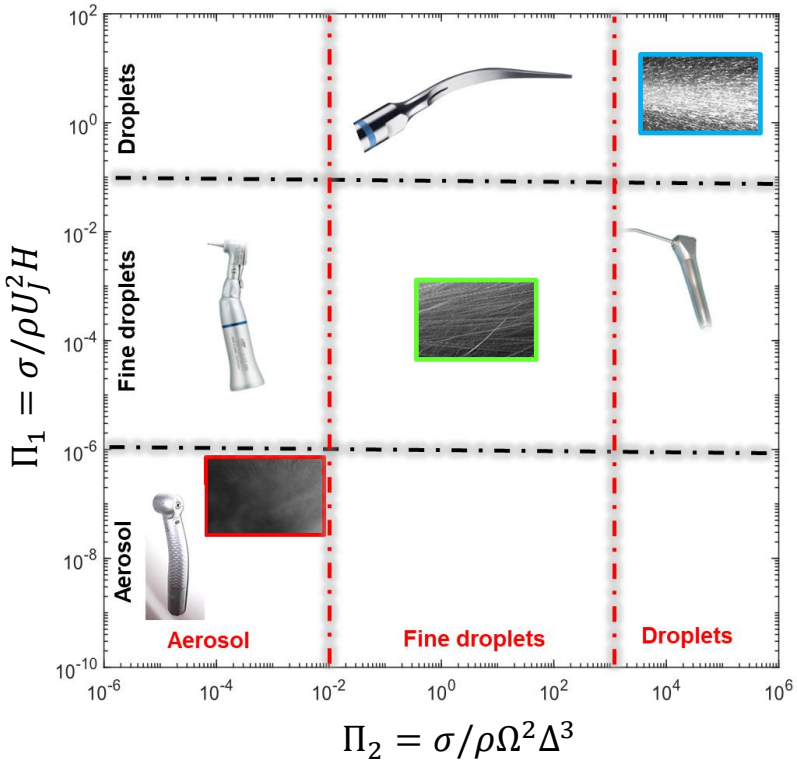

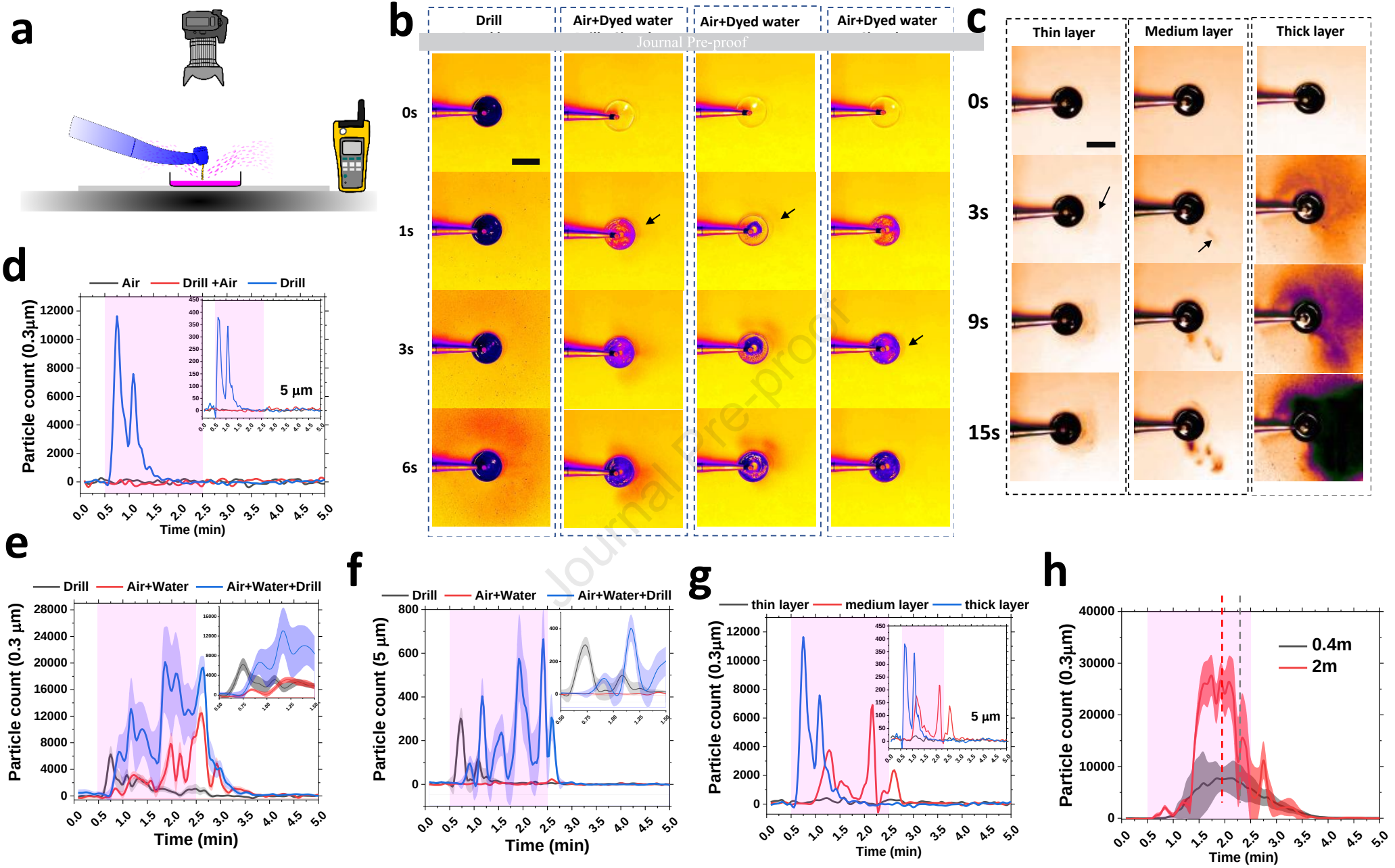

a

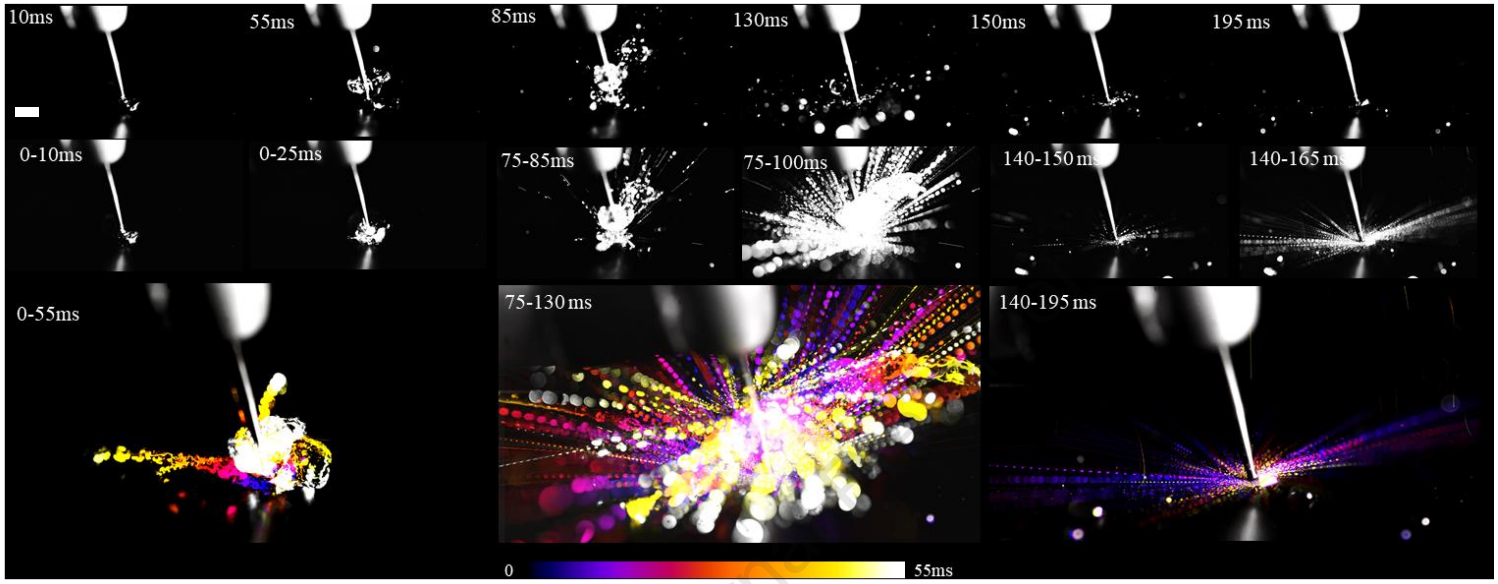
10ms
55ms
85ms
130ms
150ms
195 ms
0-10ms
0-25ms
75-85ms
75-100ms
140-150 ms
140-165 ms
0-55ms
75-130 ms
140-195 ms
0
55ms

b

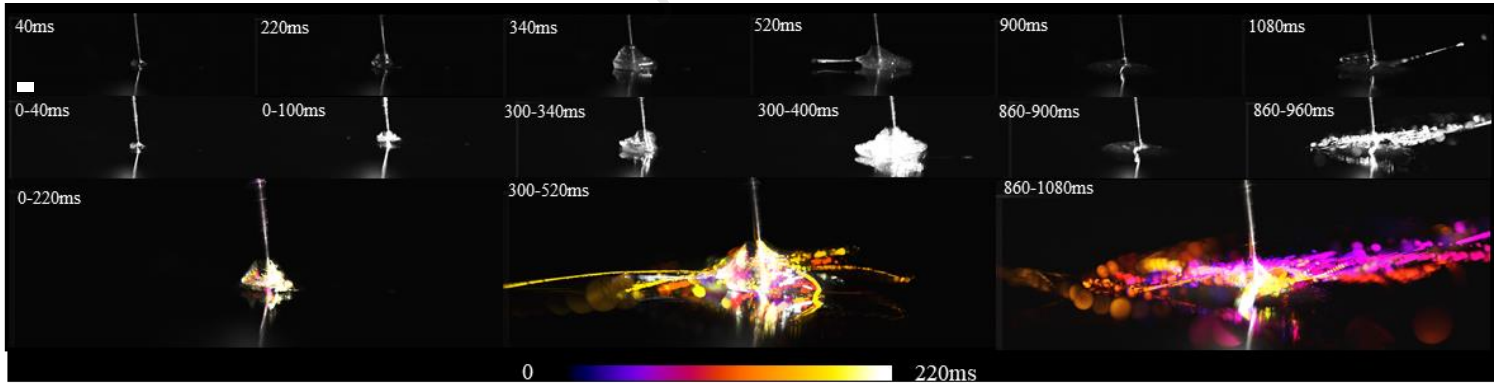
40ms
220ms
340ms
520ms
900ms
1080ms
0-40ms
0-100ms
300-340ms
300-400ms
860-900ms
860-960ms
0-220ms
300-520ms
860-1080ms
0
220ms

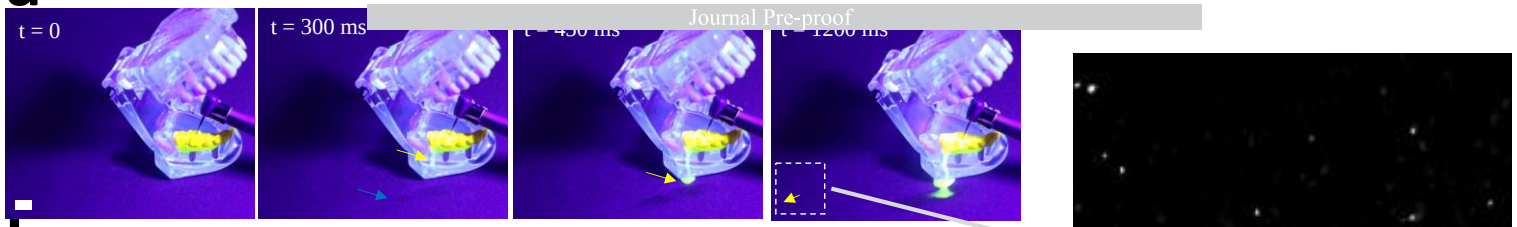

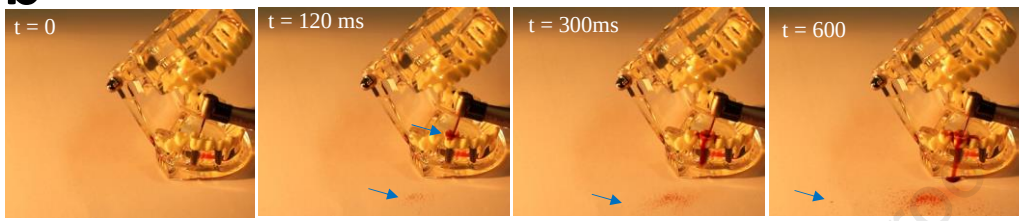

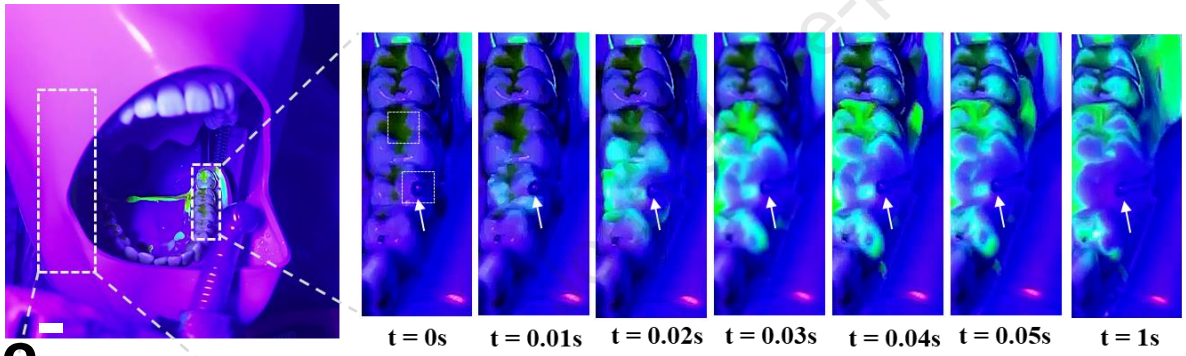

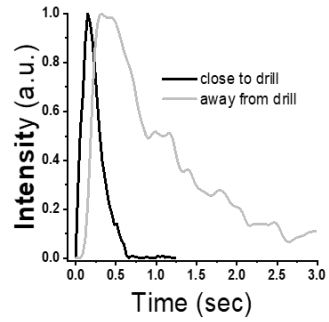

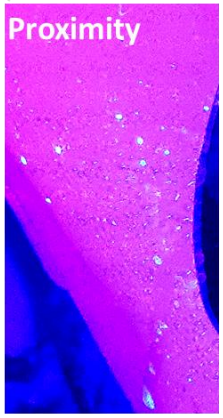

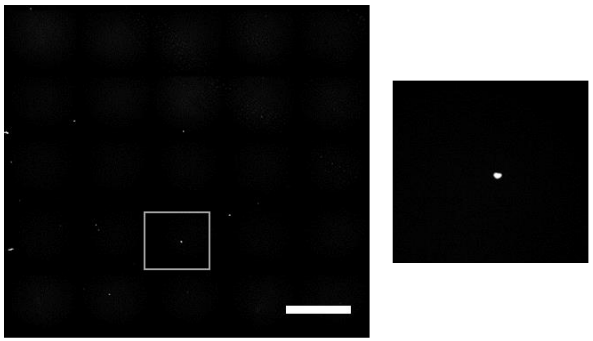

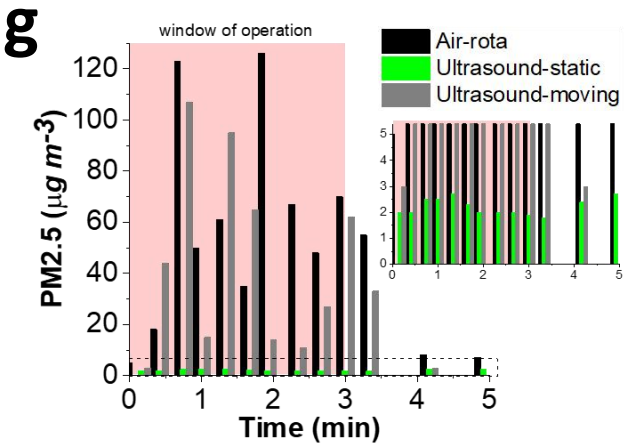

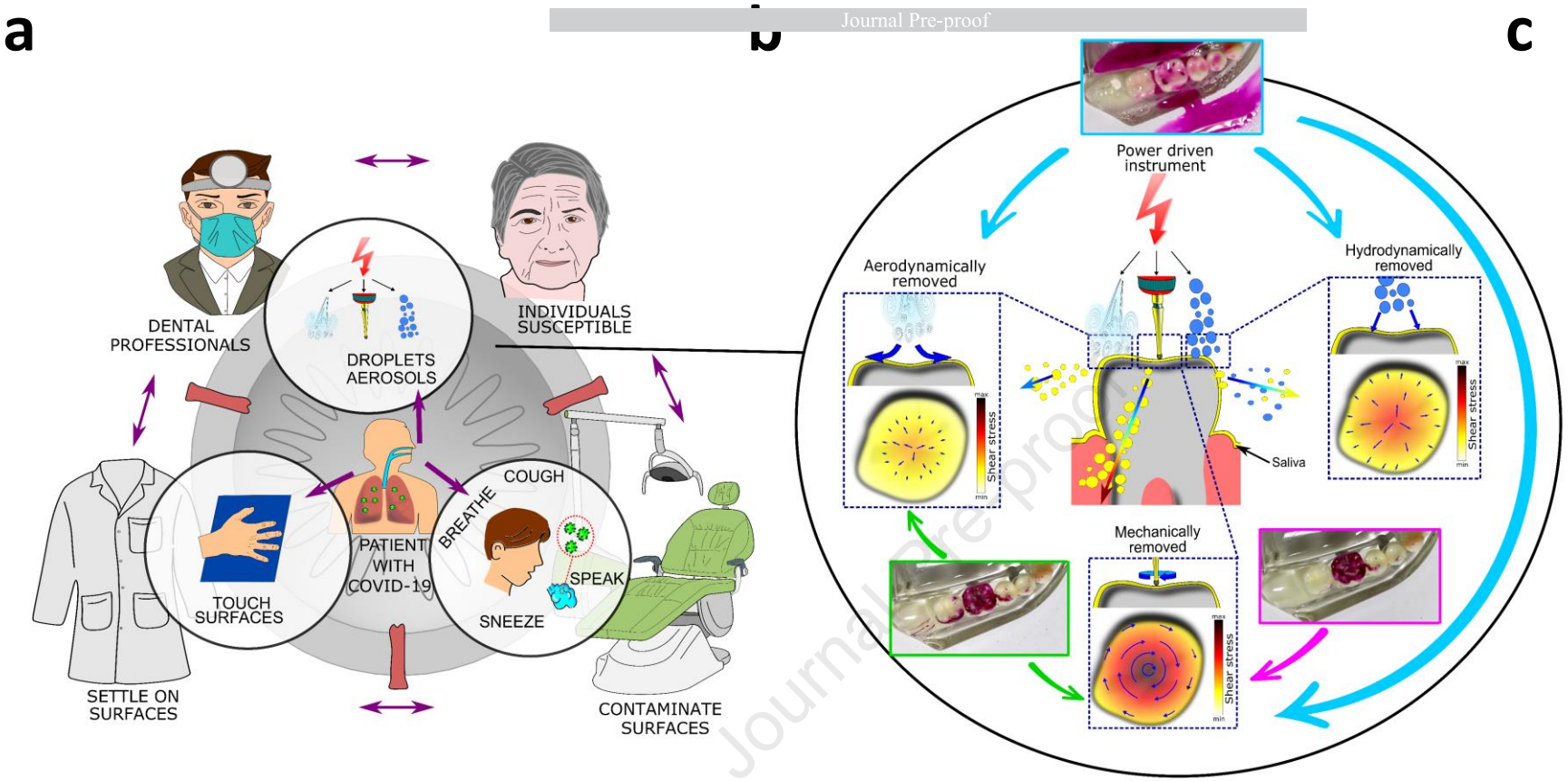

- Mechanical, hydrodynamic, and aerodynamic forces drive removal/ dispersal processes
- The air-rotor has the highest ability to remove and disperse infectious agents
- The aerosol cloud flows as a current and continuously settles
- Manipulating rheological properties of the fluids can suppress aerosol generation